

## Mechanical property changes in porous low-k dielectric thin films during processing

G. Stan, R. S. Gates, P. Kavuri, J. Torres, D. Michalak, C. Ege, J. Bielefeld, and S. W. King

Citation: [Applied Physics Letters](#) **105**, 152906 (2014); doi: 10.1063/1.4898351

View online: <http://dx.doi.org/10.1063/1.4898351>

View Table of Contents: <http://scitation.aip.org/content/aip/journal/apl/105/15?ver=pdfcov>

Published by the [AIP Publishing](#)

---

### Articles you may be interested in

[Elastic properties of porous low-k dielectric nano-films](#)

J. Appl. Phys. **110**, 043520 (2011); 10.1063/1.3624583

[The role of ultraviolet radiation during ultralow k films curing: Strengthening mechanisms and sacrificial porogen removal](#)

J. Appl. Phys. **102**, 094107 (2007); 10.1063/1.2805451

[Dependences of Young's modulus of porous silica low dielectric constant films on skeletal structure and porosity](#)

J. Appl. Phys. **100**, 123512 (2006); 10.1063/1.2401660

[Brillouin light scattering studies of the mechanical properties of ultrathin low- k dielectric films](#)

J. Appl. Phys. **100**, 013507 (2006); 10.1063/1.2209428

[Structural characterization of a porous low-dielectric-constant thin film with a non-uniform depth profile](#)

Appl. Phys. Lett. **81**, 607 (2002); 10.1063/1.1495079

---

An advertisement for Asylum Research Cypher AFMs. The background is dark blue with a glowing effect. On the left, there is a stylized image of a film strip and a purple, porous-looking structure. The text is in white and orange. The main text reads: 'Not all AFMs are created equal', 'Asylum Research Cypher™ AFMs', and 'There's no other AFM like Cypher'. At the bottom, there is a website URL: 'www.AsylumResearch.com/NoOtherAFMLikeIt' and the Oxford Instruments logo with the tagline 'The Business of Science®'.

# Mechanical property changes in porous low- $k$ dielectric thin films during processing

G. Stan,<sup>1,a)</sup> R. S. Gates,<sup>1</sup> P. Kavuri,<sup>2</sup> J. Torres,<sup>3</sup> D. Michalak,<sup>3</sup> C. Ege,<sup>3</sup> J. Bielefeld,<sup>3</sup> and S. W. King<sup>3</sup>

<sup>1</sup>Material Measurement Laboratory, National Institute of Standards and Technology, Gaithersburg, Maryland 20899, USA

<sup>2</sup>Physical Measurement Laboratory, National Institute of Standards and Technology, Gaithersburg, Maryland 20899, USA

<sup>3</sup>Logic Technology Development, Intel Corporation, Hillsboro, Oregon 97124, USA

(Received 15 August 2014; accepted 4 October 2014; published online 15 October 2014)

The design of future generations of Cu-low- $k$  dielectric interconnects with reduced electronic crosstalk often requires engineering materials with an optimal trade off between their dielectric constant and elastic modulus. This is because the benefits associated with the reduction of the dielectric constant by increasing the porosity of materials, for example, can adversely affect their mechanical integrity during processing. By using load-dependent contact-resonance atomic force microscopy, the changes in the elastic modulus of low- $k$  dielectric materials due to processing were accurately measured. These changes were linked to alterations sustained by the structure of low- $k$  dielectric films during processing. A two-phase model was used for quantitative assessments of the elastic modulus changes undergone by the organosilicate skeleton of the structure of porous and pore-filled dielectrics. © 2014 AIP Publishing LLC. [<http://dx.doi.org/10.1063/1.4898351>]

The continuous miniaturization of future integrated circuits (ICs) poses technological challenges for today's nanoscale material property characterization.<sup>1</sup> This is because, in addition to dimensional metrology, material property measurements (mechanical, electrical, magnetic, etc.) were identified as necessary control parameters to achieve the nanoscale material integration and functionality required in the next generations of ICs. As an example, in current semiconductor manufacturing, the challenge in reducing the crosstalk that hinders the performance of devices is to incorporate materials with smaller and smaller dielectric constant,<sup>2-4</sup> which are referred to as low- $k$  dielectric materials. However, as these materials are engineered to reduce their dielectric constant by introducing porosity (voids or holes), the mechanical properties degrade to the point of failure during processing.<sup>5</sup> It is thus most convincing to demonstrate reliable quantitative mechanical property measurements on specimens comparable in terms of dimensions and structure with those used in fabrication.

In this work, we detailed the change in the elastic properties of porous SiOC:H, a low- $k$  dielectric material, at a few important processing stages: SiOC:H with porogen (pore making particle) still incorporated, porous (porogen-free) SiOC:H, and polymer-filled SiOC:H. While the first two stages are routinely used in today's technology to define the porous structure that reduces the dielectric constant of materials, the polymer-filled structure is a relatively new protective strategy<sup>6</sup> to increase the mechanical stiffness of porous materials during processing. The elastic modulus of the investigated SiOC:H blanket films was measured by load-dependent contact-resonance atomic force microscopy

(CR-AFM), in a versatile and high-resolution measurement procedure. The measurements were used in a two-phase composite model to establish mechanical property-structure relationships of the materials studied and provide guidance in the controlled design and process optimization of integrated porous low- $k$  dielectrics.

The films investigated in this work were deposited by plasma enhanced chemical vapor deposition on Si(100) wafers from various combinations of alkoxysilane, helium, oxidizers, and porogens at temperatures around 250 °C. In some of the films, porosity was generated by removing the incorporated porogen through either an atomic hydrogen cure from a remote H<sub>2</sub>/He plasma at 275 °C and 50 Pa (treatment referred to as ash cure) and/or a UV cure from an industrial broad band UV source at 400 °C. Some of the processing steps and material properties of these films are summarized in Table I. As a result of plasma copolymerization, sample S1 contained porogen incorporated into the starting organosilicate structure. However, as subjected to various post-treatments (ash and/or UV cures), the

TABLE I. Description and some material properties of the SiOC:H films investigated in this work;  $h$  and  $k$  refer here to thickness and dielectric constant of the films, respectively. The measurement uncertainty for porosity was within  $\pm 2\%$  and for the dielectric constant  $\pm 0.1\%$ .

Sample	Composition	Ash	UV	$h$ (nm)	Porosity (%)	$k$
1	With porogen	No	No	120	4	2.9
2	Porogen-free	Yes	No	110	48	2.0
3	Porogen-free	No	Yes	95	33	2.3
4	Porogen-free	Yes	Yes	90	45	2.0
5	HP-filled	Yes	Yes	78	3	3.0
6	Non-porogen	No	No	200	2	3.2
7	Non-porogen	No	Yes	200	0	3.2

<sup>a)</sup>Also at Department of Mechanical Engineering, University of Maryland, College Park, Maryland 20742, USA. Electronic mail: gheorge.stan@nist.gov.

organosilicate skeleton of the porous films (samples S2 to S5) underwent alterations from its initial structural cross-linkage and porosity. Additionally, the pores of sample S5 were filled back in with a hydrocarbon polymer (HP) by spin-coating the polymer on top of the film and heating the wafer at temperatures above the glass temperature of the HP. With all these processes, only samples S4 and S5 can be considered as having the same chemical (cross-linkage) and physical (pore morphology) organosilicate skeleton. Finally, for comparison purposes, the mechanical properties of the organosilicate skeleton were directly probed on uncured (sample S6) and UV cured (sample S7) non-porogen (no porogen added) SiOC:H films.

The elastic modulus measurements were made by load-dependent CR-AFM,<sup>7,8</sup> previously developed for monitoring the change in the resonance frequency of a cantilever eigenmode when an AFM probe is brought in and out of contact with a material. For the maximum applied load of 50 nN used in these measurements, it has been found that on any of the materials tested, sweeps between 950 kHz and 1200 kHz provided a common range for observing the shifts in the resonance frequency of the second eigenmode of the cantilever; a number of at least ten measurements were made on each sample. The first two free eigenmode frequencies of the AFM probe used (NCL-R150 probes from NanoSensors, Neuchatel, Switzerland<sup>9</sup>) were 161.0 kHz and 996.8 kHz, respectively, and the cantilever intrinsic stiffness was  $34.2 \text{ N/m} \pm 0.3 \text{ N/m}$ , as measured by laser-Doppler vibrometer (Polytec, GmbH, Waldbronn, Germany).<sup>9-11</sup> A flat-punch contact geometry was realized in these measurements by pre-flattening the apex of the tip<sup>12</sup> on a flat Si surface at loads about 100 nN higher than the maximum applied force used during measurements. The flat-punch characteristic response can be easily observed in the contact part of the measurements, as shown in Fig. 1 for samples S4 and S5. Thus, the constant contact area established during the full contact between the flat-punch and the sample surface, on both approach and retract, is indicated by the unchanging

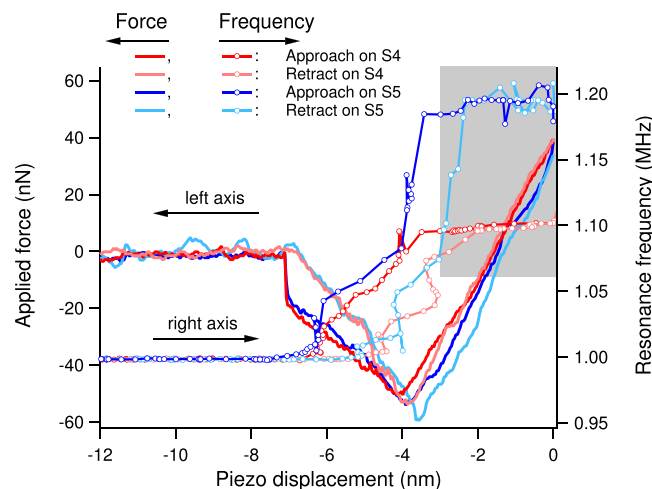


FIG. 1. Force and resonance frequency responses of an AFM cantilever during in and out-of-contact ramps on samples S4 and S5; each ramp was completed in 100 s. The gray area highlights the region where the full contact between the flat-punch and the sample surface is realized; this is the contact region where the intrinsic elasticity of each material distinctively modifies the static and dynamic mechanical response of the cantilever.

contact resonance frequency within a range of applied forces (the gray area in Fig. 1). This predefined flat-punch contact configuration provided both an improved repeatability and reliability of measurements and an increased measurement sensitivity. The measured contact resonance frequencies were converted into tip-sample contact stiffnesses by using the dynamic spring-coupled cantilever beam model.<sup>14</sup>

The continuous variation in contact stiffness as the tip was brought in and out of contact is shown in Fig. 2 for samples S4 and S5 and a polystyrene (PS) film (used also as an elastic modulus calibration reference for CR-AFM measurements<sup>12</sup>). It is observed that the contact stiffness increases as the contact is progressively established when the tip snaps into contact (negative values of the applied force); the reverse behavior occurs in the same range of applied forces when the tip is retracted and the contact stiffness decreases to zero. However, once a full contact is established between the flattened part of the tip and the sample surface, no notable variation is exhibited by the contact stiffness in the range of positive applied forces (refer to the gray area in Fig. 2). The contact stiffness,  $k^*$ , and the reduced tip-sample elastic modulus,  $E^*$ , are related by<sup>15</sup>  $k^* = 2aE^*$ , where  $a$  is the contact radius and  $1/E^* = 1/M_S + 1/M_T$ , with  $M_S$  and  $M_T$  being the indentation moduli of the sample and tip, respectively. In the case of an elastically isotropic material, the indentation modulus is defined as  $M = E/(1 - \nu^2)$ , with  $E$  being the Young's modulus and  $\nu$  being the Poisson's ratio of the material.

Qualitatively, from the full-contact region of the measurements shown in Fig. 2, a significant increase in the elastic modulus of sample S5 is observed with respect to that of sample S4, with PS in between these two. Quantitatively, the plateaued contact stiffness values  $k_S^*$  from the full-contact region can be used to calculate the indentation moduli  $M_S$  of the samples probed. The indentation modulus of each sample was determined from the measured contact stiffness and radius of the flat end of the tip (SEM images of the tip are shown in Ref. 12) and further deconvolution of the contributions to  $M_S$  was made to extract the Young's modulus of each

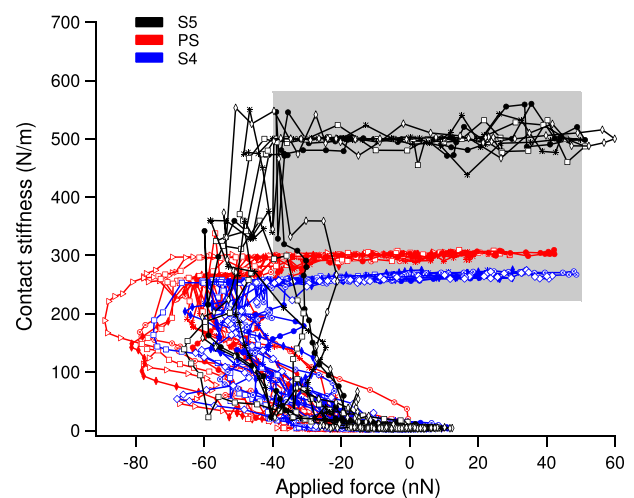


FIG. 2. Contact stiffness versus applied force at contacts on sample S4, sample S5, and PS film. The measurements were randomly alternated on these three samples to attest the invariability of contact geometry. The gray area highlights the same full-contact region shown in Fig. 1.

film by using the Xu and Pharr contact model<sup>13</sup> for a coated substrate indented by a flat punch. The substrate contribution to the elastic moduli of the samples (substrate + film)<sup>12</sup> was found to be within 30% for these measurements.

The values obtained for the Young's moduli of the investigated films are shown in Fig. 3 and Table SI<sup>12</sup> as a function of porosity; they were calculated from the determined indentation moduli and an average Poisson's ratio of 0.25.<sup>16,17</sup> Although in films as thick as 800 nm UV curing has been shown to nonuniformly alter the material properties across the film thickness,<sup>18</sup> it is likely that a more homogeneous curing took place within the thickness of our 100 nm thick films. Additionally, by considering the invariance of the contact stiffness with depth and the necessity of substrate correction, the elastic modulus values reported here are representative for the mean values across the thickness of the films. The effects of the ash and UV cures are observed in the elastic moduli of the cured porous films by comparing them with the elastic modulus of the starting sample S1. Thus, the ash cure, used to promote a more efficient porogen removal,<sup>19</sup> produces a significant decrease in the elastic modulus from 4.2 GPa to 1.6 GPa (from S1 to S2) along with the porogen removal. Similar damaging effect of ashing on the mechanical properties of porous low-*k* dielectrics was assessed previously by nanoindentation but only in qualitative terms due to the unavoidable substrate contribution to the elastic modulus measurements.<sup>19</sup> On the other hand, the effect of UV is to remove the porogen and enhance the mechanical rigidity of the structure by enriching the Si-O-Si cross-linking.<sup>20</sup> The UV cure also leads to a film shrinkage along with either an increase in porosity (porogen removal and bond reorganization when no ash cure is applied) or a decrease in porosity (porogen removal, if any, and bond reorganization after an ash cure). Regarding the mechanical

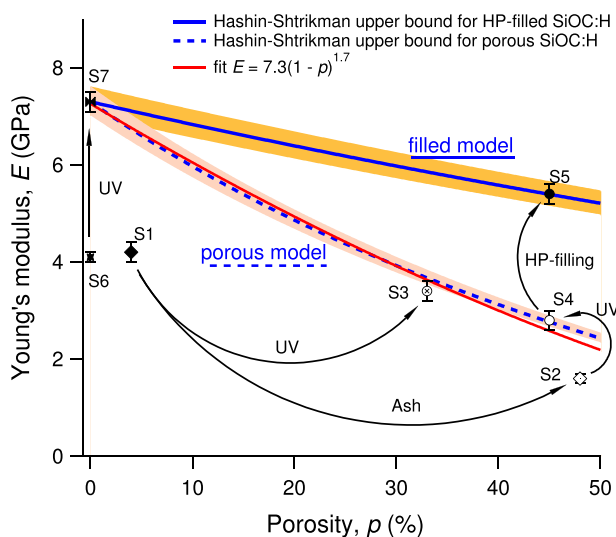


FIG. 3. Elastic moduli of SiOC:H films of various porosity and composition. The Hashin-Shtrikman model was used to fit the elastic moduli of filled (blue continuous line) and unfilled (blue dotted line) porous SiOC:H films that have skeleton structures with the same mechanical stiffness as the non-porous sample S7. The yellow and pink zones cover the maximum uncertainty generated in the model by the fit uncertainties; all the measurement uncertainties represent one standard deviation of the measured values. The red line represents a simple porous model fit (solid fraction at 1.7 power) as a comparison.

properties, the UV cure mitigates the loss in rigidity due to the increase in porosity by increasing the stiffness of the organosilicate skeleton. In both cases shown in Fig. 3, with porogen partially (from S1 to S3) or fully (from S2 to S4) removed, the stiffening effect of UV on the organosilicate skeleton is demonstrated. The same effect of UV on the stiffness of the organosilicate skeleton was observed also in the case of non-porogen SiOC:H films, with an increase in the elastic modulus from 4.1 GPa (sample S6) to 7.3 GPa (sample S7). The effect of ashing can be assessed also from the difference between samples S3 and S4 in terms of porosity increase (from 33% to 45%) and elastic modulus reduction (from 3.4 GPa to 2.8 GPa). By considering that the effect of UV curing on the stiffness of the organosilica skeleton is independent of porosity,<sup>21</sup> this difference in the elastic moduli of sample S3 and S4 could be entirely ascribed to the removal of porogen residuals from the pores of sample S4. Similar effects of ash and broad-band UV cures on the mechanical properties of SiOC:H porous films were reported previously in nanoindentation measurements.<sup>22</sup>

From the above analysis, it can be concluded that only samples S4 and S5 can be considered as having organosilicate skeletons with the same pore morphology and mechanical stiffness: S4 with non-filled pores and S5 with HP-filled pores. Also, as the result of UV curing, the stiffness of their skeletons matches with that of sample S7. Therefore, a consistent property-structure analysis had to be restricted to S4, S5, and S7 films only and it was done based on the Hashin-Shtrikman model<sup>23</sup> for the effective elastic modulus of a multiphase composite material. In the limits of the Hashin-Shtrikman model, the structure of the porous films was considered as consisting of a solid skeleton (organosilica phase) with either empty (void phase) or filled (HP phase) spherical inclusions. For these two cases, the measurements were simultaneously fitted<sup>12</sup> by the upper bound of the model and the fit results are shown in Fig. 3 with blue lines: the continuous blue line fits the measurements on samples S5 and S7 and the dotted line fits the measurements on samples S4 and S7. The fits predicted  $7.3 \pm 0.3$  GPa and  $3.6 \pm 0.2$  GPa for the elastic moduli of the skeleton and filling polymer, respectively, which are in very good agreement with the corresponding measured elastic moduli:  $7.3 \pm 0.2$  GPa on sample S7 and  $3.3 \pm 0.1$  GPa on a separate blanket film of HP. Even though, as pointed out above, the pores of S3 are not entirely empty, its elastic modulus comes closed to the theoretical limit of the model, suggesting that the elastic modulus of the skeleton of this film is quite similar with those of S4 and S5. The results demonstrate good quantitative agreement of the measured and calculated moduli for the porous, filled, and matrix of SiOC:H materials and indicate that polymer filling of porous dielectrics is a viable strategy for improving the mechanical rigidity of these materials during processing. Shielding the porosity during processing has been shown to provide substantial protection of the porous materials from plasma-induced damages in terms of etch control and geometrical aspect ratio.<sup>6</sup>

In terms of relative values,  $E_{\text{porous}}/E_{\text{skeleton}}$  versus porosity  $p$ , the observed porosity dependence of the elastic modulus of the unfilled porous films corresponds to a reduction of about 70% in the elastic modulus at 50% porosity. This

dependence roughly approximates the power-law decaying for foam materials,<sup>24–26</sup>  $E_{\text{porous}}/E_{\text{skeleton}} \approx (1-p)^n$ , with  $n$  approaching 1.7 for the fit of samples S7, S3, and S4 (red curve in Fig. 3). Such rather mild decay ( $n < 2$ ) of the elastic modulus with porosity correlates with a microstructure that consists of moderately overlapping spherical pores;<sup>24</sup> more severe decays, about 80% in the case of overlapping spherical pores and 90% in the case of overlapping solid sphere, have been calculated and reported at 50% porosity.<sup>21,27,28</sup> It should be noted that in our case, the small operational indentation depths (several nanometers) prevent any structural changes during measurements; however, this is not the case of instrumented nanoindentation, which normally operates in the range of tens of nanometers and, in which case, substrate effects and changes in the porous microstructure during indentation complicate the interpretation of measurements.<sup>29,30</sup> Typically, an overestimation of 2 GPa to 3 GPa for the elastic moduli of low- $k$  ultrathin film has been observed when nanoindentation measurements without substrate correction were compared with other nanoscale elastic modulus measurement techniques like Brillouin light scattering<sup>17</sup> and CR-AFM.<sup>12</sup>

In summary, in this work, we have demonstrated reliable and highly sensitive elastic modulus measurement of low- $k$  dielectric thin films. The adapted load-dependence CR-AFM technique with pre-flattened tips provided a direct and easy procedure to quantitatively determine the elastic modulus of thin films with nanoscale spatial resolution. The measurements were used to assess the effect of technological processes (ash and UV cures and pore filling) on the elastic modulus of these films and deconvolute the contributions of the constituents to the elastic modulus of each film. Furthermore, the elastic moduli of filled and unfilled porous films were compared to probe the efficacy of pore filling and analyze the structure-property relationship of these materials.

<sup>1</sup>S. W. King, H. Simka, D. Herr, H. Akinaga, and M. Garner, *APL Mater.* **1**, 040701 (2013).

<sup>2</sup>K. Maex, M. R. Baklanov, D. Shamiryan, F. Iacopi, S. H. Brongersma, and Z. S. Yanovitskaya, *J. Appl. Phys.* **93**, 8793 (2003).

<sup>3</sup>W. Volksen, R. D. Miller, and G. Dubois, *Chem. Rev.* **110**, 56 (2010).

<sup>4</sup>G. Dubois and W. Volksen, in *Advanced Interconnects for ULSI Technology*, edited by M. R. Baklanov, P. S. Ho, and E. Zschech, (Wiley Online Library, 2012), pp. 1–33.

<sup>5</sup>M. R. Baklanov, J.-F. de Marneffe, D. Shamiryan, A. M. Urbanowicz, H. Shi, T. V. Rakhimova, H. Huang, and P. S. Ho, *J. Appl. Phys.* **113**, 041101 (2013).

<sup>6</sup>T. Frot, W. Volksen, S. Purushothaman, R. Bruce, and G. Dubois, *Adv. Mater.* **23**, 2828–2832 (2011).

<sup>7</sup>G. Stan, S. W. King, and R. F. Cook, *J. Mater. Res.* **24**, 2960 (2009).

<sup>8</sup>G. Stan, S. D. Solares, B. Pittenger, N. Erina, and C. Su, *Nanoscale* **6**, 962 (2014).

<sup>9</sup>Any mention of commercial products in this paper is for information only; it does not imply recommendation or endorsement by NIST.

<sup>10</sup>R. S. Gates and J. R. Pratt, *Nanotechnology* **23**, 375702 (2012).

<sup>11</sup>R. S. Gates, W. A. Osborn, and J. R. Pratt, *Nanotechnology* **24**, 255706 (2013).

<sup>12</sup>See supplementary material at <http://dx.doi.org/10.1063/1.4898351> for contact geometry characterization and fit procedure for the porosity dependence of the elastic moduli of low- $k$  dielectric films.

<sup>13</sup>H. Xu and G. M. Pharr, *Scr. Mater.* **55**, 315 (2006).

<sup>14</sup>U. Rabe, K. Janser, and W. Arnold, *Rev. Sci. Instrum.* **67**, 3281 (1996).

<sup>15</sup>K. L. Johnson, *Contact Mechanics* (Cambridge University Press, Cambridge, 1985).

<sup>16</sup>W. Zhou, S. Bailey, R. Sooryakumar, S. King, G. Xu, E. Mays, C. Ege, and J. Bielefeld, *J. Appl. Phys.* **110**, 043520 (2011).

<sup>17</sup>S. Bailey, E. Mays, D. J. Michalak, R. Chebiam, S. King, and R. Sooryakumar, *J. Phys. D: Appl. Phys.* **46**, 045308 (2013).

<sup>18</sup>A. M. Lomonosov, A. Ayouch, P. Ruello, G. Vaudel, M. R. Baklanov, P. Verdonck, L. Zhao, and V. E. Gusev, *ACS Nano* **6**, 1410 (2012).

<sup>19</sup>A. M. Urbanowicz, K. Vanstreels, D. Shamiryan, S. De Gendt, and M. R. Baklanov, *Electrochem. Solid-State Lett.* **12**, H292 (2009).

<sup>20</sup>F. Iacopi, Y. Travaly, B. Eyckens, C. Waldfried, T. Abell, E. P. Guyer, D. M. Gage, R. H. Dauskardt, T. Sajavaara, K. Houthoofd, P. Grobet, P. Jacobs, and K. Maex, *J. Appl. Phys.* **99**, 053511 (2006).

<sup>21</sup>K. Vanstreels, C. Wu, P. Verdonck, and M. R. Baklanov, *Appl. Phys. Lett.* **101**, 123109 (2012).

<sup>22</sup>A. M. Urbanowicz, K. Vanstreels, P. Verdonck, E. Van Besien, T. Christos, D. Shamiryan, S. De Gendt, and M. R. Baklanov, *J. Vac. Sci. Technol., B* **29**, 032201 (2011).

<sup>23</sup>Z. Hashin and S. Shtrikman, *J. Mech. Phys. Solids* **11**, 127–140 (1963).

<sup>24</sup>A. Jain, S. Rogojevic, W. N. Gill, J. L. Plawsky, I. Matthew, M. Tomozawa, and E. Simonyi, *J. Appl. Phys.* **90**, 5832 (2001).

<sup>25</sup>G. Dubois, W. Volksen, T. Magbitang, R. D. Miller, D. M. Gage, and R. H. Dauskardt, *Adv. Mater.* **19**, 3989 (2007).

<sup>26</sup>H. Fan, C. Hartshorn, T. Buchheit, D. Tallant, R. Assink, R. Simpson, D. J. Kissel, D. J. Lacks, S. Torquato, and C. J. Brinker, *Nat. Mater.* **6**, 418 (2007).

<sup>27</sup>H. Li, Y. Lin, T. Y. Tsui, and J. J. Vlassak, *J. Mater. Res.* **24**, 107 (2009).

<sup>28</sup>K. B. Yeap, M. Kopycinska-Müller, L. Chen, Y. Chen, M. Jungmann, R. Krause-Rehberg, S. Mahajan, J. Vlassak, M. Gall, and E. Zschech, *J. Mater. Res.* **28**, 1262 (2013).

<sup>29</sup>M. Kopycinska-Müller, K. B. Yeap, S. Mahajan, B. Köhler, N. Kuzeyeva, T. Müller, E. Zschech, and K. J. Wolter, *Nanotechnology* **24**, 355703 (2013).

<sup>30</sup>X. Chen, Y. Xiang, and J. J. Vlassak, *J. Mater. Res.* **21**, 715 (2006).